JACS
JOURNAL OF THE AMERICAN CHEMICAL SOCIETY

Communication

pubs.acs.org/JACS

β-Ketoenamine-Linked Covalent Organic Frameworks Capable of Pseudocapacitive Energy Storage

Catherine R. DeBlase, Katharine E. Silberstein, Thanh-Tam Truong, Héctor D. Abruña, and William R. Dichtel*

Department of Chemistry and Chemical Biology, Cornell University, Baker Laboratory, Ithaca, New York 14853-1301, United States

Supporting Information

ABSTRACT: Two-dimensional covalent organic frameworks (2D COFs) are candidate materials for charge storage devices because of their micro- or mesoporosity, high surface area, and ability to predictably organize redox-active groups. The limited chemical and oxidative stability of established COF linkages, such as boroxines and boronate esters, precludes these applications, and no 2D COF has demonstrated reversible redox behavior. Here we describe a β-ketoenamine-linked 2D COF that exhibits reversible electrochemical processes of its anthraquinone subunits, excellent chemical stability to a strongly acidic electrolyte, and one of the highest surface areas of the imine- or enamine-linked 2D COFs. Electrodes modified with the redox-active COF show higher capacitance than those modified with a similar non-redox-active COF, even after 5000 charge−discharge cycles. These findings demonstrate the promise of using 2D COFs for capacitive storage.

High surface area electrodes provide sensing platforms,[1] electrocatalyst supports,[2] and improved energy storage and conversion devices,[3] including batteries,[4] supercapacitors,[5,6] and fuel cells.[7] In contrast to many previous strategies for accessing meso- and microporous electrodes,[6,8] framework materials, such as metal−organic frameworks (MOFs) and covalent organic frameworks (COFs), offer uniform nanometer-scale pores and predictive design criteria to organize functional building blocks. COFs, which are crystalline polymer networks comprised of light elements,[9,10] adopt two-dimensional (2D) layered structures with high spectroscopic charge-carrier mobilities.[11] However, characterizing these properties electrochemically or utilizing COFs in electrochemical devices has been hampered by the poor hydrolytic and oxidative stability of boronate ester-linked frameworks that dominated the early COF literature.[10] Here we incorporate redox-active 2,6-diaminoanthraquinone (**DAAQ**) moieties into a 2D COF linked by β-ketoenamines, which were shown by Banerjee et al. to confer outstanding hydrolytic stability.[12,13] This material is the first COF to exhibit well-defined, rapid redox processes, which we attribute to its 2D layered architecture as well as increased capacitance relative to both its electroactive monomer and a COF lacking redox-active groups. We also developed improved conditions for β-ketoenamine COF synthesis, such that the surface area of the **DAAQ-TFP COF** is among the highest of all COFs linked by either imines or enamines. These findings demonstrate the promise of these robust COFs as electrode materials, particularly as methods emerge to incorporate them into devices as large-area crystalline thin films[14] instead of as the polycrystalline powders accessed thus far.

The layered sheets of 2D COFs typically adopt nearly eclipsed stacked structures, providing continuous nanometer-scale channels normal to the stacking direction as well as significant π-orbital overlap between monomers in adjacent layers. These features provide an accessible high surface area interface for double-layer formation and pathways for charge transfer to/from redox-active groups that comprise the walls. Here, **DAAQ** moieties, which are reduced to 9,10-dihydroxyanthracenes upon two-electron, two-proton reduction in a protic electrolyte, serve this function. The remarkable stability of β-ketoenamine-linked COFs, even to 1 M H_2SO_4, makes them ideally suited for these studies. These COFs are formed by condensing polyfunctional anilines with 1,3,5-triformylphloroglucinol (**TFP**, **3**), and their exceptional hydrolytic stability was attributed to the irreversible tautomerization of their initially formed imines.[12] However, irreversible condensation reactions provide amorphous polymer networks, not crystalline COFs. To reconcile this apparent contradiction, we found that free anilines exchange into preformed tris(β-ketoenamine) model compounds (see Supporting Information, SI), which provides the dynamic bond exchange thought to be needed for COF crystallization.

Both the **DAAQ-** and **DAB-TFP COF** were obtained by condensing either **DAAQ 1** or *p*-diaminobenzene (**DAB**) **2** with **TFP 3** under solvothermal conditions (Figure 1). The FTIR spectra (Figure S4) of the powders show the disappearance of the N−H stretch as well as the emergence of a new C−N stretch at 1250 cm^{-1}. This resonance is characteristic of β-ketoenamine C−N moieties and appears in the spectrum of the model compound **S1** (Figure S4), whose structure was confirmed by NMR spectroscopy.[15] The C═O stretch of **3** (1658 cm^{-1}) also shifts to a lower energy characteristic of the β−ketoenamine C═O stretch (1615 cm^{-1}). Furthermore, the spectra of both model **S1** and the isolated powders lack OH stretches that would be expected for species comprised of imine tautomers. ^{13}C cross-polarization magic angle spinning (CP-MAS) solid-state NMR spectroscopy also indicated the formation of β-ketoenamine-linked materials, as the spectra of both **DAAQ-** and **DAB-TFP COF** exhibit resonances at 145 ppm that are assigned to the enamine carbon (═CNH) and α-enamine carbon at 115 ppm (Figure S8).[12] Furthermore, the **TFP** aldehyde resonance at 193

Received: September 11, 2013
Published: October 22, 2013

dx.doi.org/10.1021/ja409421d | J. Am. Chem. Soc. 2013, 135, 16821−16824

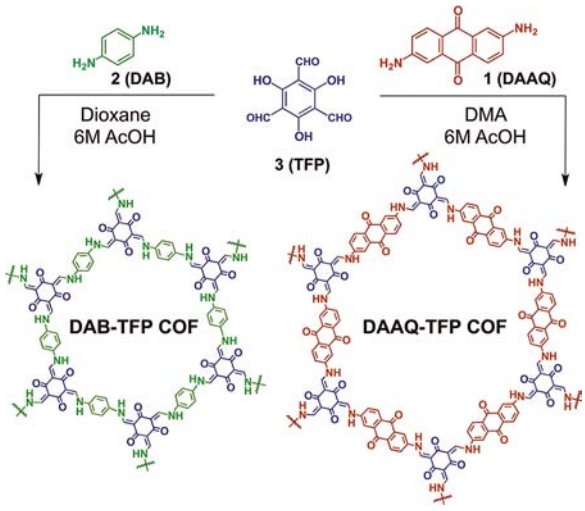

Figure 1. Synthesis of **DAB**- and **DAAQ-TFP COF**.

ppm (Figure S10) was replaced by a peak at ∼180 ppm, corresponding to a ketone resonance. High-resolution X-ray photoelectron spectroscopy also differentiates between N atoms in the different bonding environments. The two *β*-ketoenamine-linked COFs as well as model compound **S1** exhibit N_{1s} binding energies of 399.2 eV, whereas imine and aniline binding energies are typically 398.6 and 398.0 eV, respectively (Figure S11).[16] These collective observations indicate that the **DAAQ** and **DAB** monomers form similar *β*-ketoenamine-linked networks.

The two *β*-ketoenamine-linked COFs exhibit powder X-ray diffraction (PXRD) patterns that are typical of 2D layered hexagonal networks. Pawley refinement of the **DAAQ-TFP COF** using a *P6/m* unit cell matches the experimental diffraction pattern well with acceptably low residuals (R_p = 5.86%). The **DAAQ-TFP COF** exhibits an intense diffraction peak at 3.5° as well as peaks at 5.9°, 7.0°, and a broad peak at 27°, corresponding to the 100, 110, 210, and 001 reflections, respectively, of a nearly eclipsed layered structure with a pore diameter of 2.3 nm (Figure 2). The PXRD pattern of the **DAB-TFP COF** is consistent with its previous report,[12] featuring peaks at 4.7° (100), 7.8° (110), 8.5° (210), and 26.5° (001). **DAAQ-TFP COF** forms spherical particles of ∼2 *μ*m in diameter, as characterized using scanning electron microscopy (SEM) (Figure S3).

Optimization of the solvothermal growth conditions for the **DAAQ-TFP COF** provided high specific surface area materials that approached their theoretical values for the first time. We had initially synthesized **DAB-TFP COF** in dioxane, and the resulting powders exhibited Type IV N_2 adsorption isotherms corresponding to a BET surface area (S_{BET}) of 365 $m^2\ g^{-1}$. This value is comparable to the high end of the range achieved by Banerjee et al. using either grinding (35 $m^2\ g^{-1}$) or solvothermal (535 $m^2\ g^{-1}$) syntheses.[12,13] However, the Connelly surface area of **DAB-TFP COF** is 2420 $m^2\ g^{-1}$, much higher than has been demonstrated experimentally. **DAAQ-TFP COF** powders synthesized in dioxane exhibited comparable BET surface areas (435 $m^2\ g^{-1}$) as well as extra peaks in their PXRD patterns that we attributed to residual **DAAQ** monomer **1** contamination (Figure S12). We noted that **1** is poorly soluble in dioxane and instead crystallized the COF from *N*,*N*-dimethylacetamide (DMA), in which **1** showed the highest solubility during a solvent screen. The PXRD pattern of **DAAQ-TFP COF** prepared in DMA is free of monomer impurities, and the resulting samples provided S_{BET} of 1124 $m^2\ g^{-1} \pm 422$ (average of 5 samples) the highest of which was 1800 $m^2\ g^{-1}$. These values approach the Connelly surface area of the framework (2340 $m^2\ g^{-1}$) and are significantly higher than most other imine or *β*-ketoenamine-linked 2D COFs.[17] The pore size distribution of **DAAQ-TFP COF** (Figure 3B) calculated using nonlocal density functional theory was centered at 20 Å, which is reasonably close to the predicted pore size (23 Å).

The anthraquinone moieties within the **DAAQ-TFP COF** undergo reversible redox processes, such that this material is the first COF to exhibit a well-defined electrochemical response. Cyclic voltammetry (CV) of **DAAQ-TFP COF** (Figure 4) was performed by drying an *N*-methylpyrollidinone slurry of the

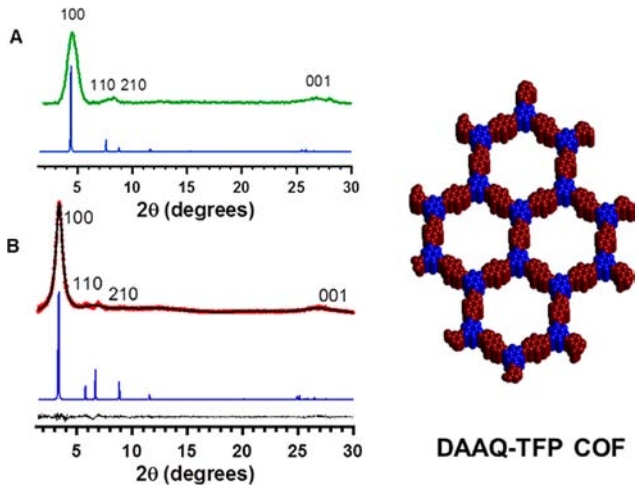

Figure 2. (A) Experimental (green) and predicted (blue) PXRD patterns of **DAB-TFP COF**. (B) Experimental (red dots), Pawley refined (superimposed black line), and predicted (blue) PXRD patterns of **DAAQ-TFP COF** and a difference plot (experimental, refined; black). Right: The extended structure of **DAAQ-TFP COF**.

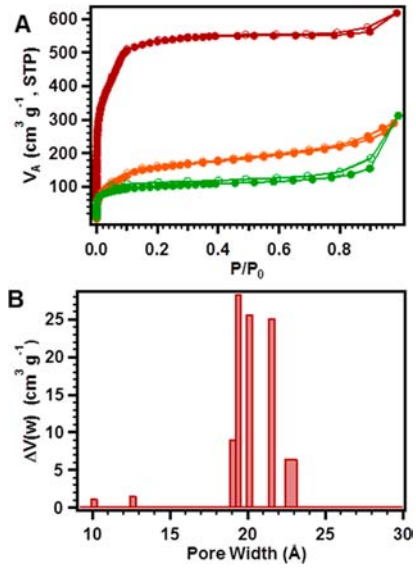

Figure 3. (A) N_2 adsorption (closed circles) and desorption (open circles) isotherms of **DAAQ-TFP COF** synthesized in DMA (red, S_{BET} = 1280 $m^2\ g^{-1}$) and dioxane (orange, S_{BET} = 435 $m^2\ g^{-1}$) and **DAB-TFP COF** synthesized in dioxane (green, S_{BET} = 365 $m^2\ g^{-1}$). (B) Pore size distribution of **DAAQ-TFP COF** synthesized in DMA.

dx.doi.org/10.1021/ja409421d | *J. Am. Chem. Soc.* 2013, 135, 16821−16824

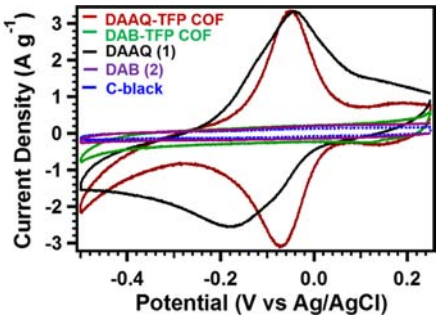

Figure 4. Cyclic voltammograms (50 mV s^{-1}, 1 M H_2SO_4 supporting electrolyte) of **DAAQ-TFP COF** (red), **DAB-TFP COF** (green), **DAAQ** monomer **1** (black), **DAB** monomer **2** (purple), and carbon black-only (blue).

COF (35 wt %), carbon black (60 wt %), and polyvinylidene fluoride (PVDF) binder (5 wt %) onto a glassy carbon (GC) electrode, which was subjected to an applied potential in a fritted three compartment cell containing 1 M H_2SO_4 supporting electrolyte (see SI for fabrication procedure). **DAAQ-TFP COF**-functionalized electrodes exhibited a reversible Faradaic process with an E° of −0.058 V vs Ag/AgCl. The peak separation (ΔE_p) between the oxidative and reductive waves was quite small (4 mV), indicative of rapid electron transfer between the GC electrode and the COF anthraquinones. In addition, the voltammetric profile was typical of a surface-confined redox couple. Moreover, the peak current was directly proportional to the scan rate over the range of 1−1000 mV sec^{-1}, consistent with the above statement (Figure S26). The rapid charge transfer is inherent to the COF architecture as the corresponding redox process of electrodes functionalized with monomer **1** exhibited a very large $\Delta E_p \approx 160$ mV, indicative of slow heterogeneous charge transfer. There is also a shift in the formal potential (E° = −0.11 V). We attribute these differences in behavior to more facile protonation of the quinone moieties during their reduction in the porous COF architecture. The voltammetric profile of the COF functionalized electrodes was symmetric with well-matched current densities (peak currents of ±3 A g^{-1} at a 50 mV s^{-1} scan rate). In contrast, electrodes containing **1** exhibited significantly broadened waves with the reduction wave shifted to more negative potentials and exhibiting a lower current density than the oxidative counterpart, suggesting both kinetic limitations and coupled chemical reactions.

The high surface area and reversible redox processes of the **DAAQ-TFP COF** are of interest for pseudocapacitive energy storage devices, in which charge is stored both in the electrochemical double layer and through surface-bound Faradaic (pseudocapacitive) processes. The double-layer capacitance of a material is directly proportional to its electroactive surface area, which depends on the surface area of the material and its conductivity. Faradaic charge transfer to/from redox-active COFs provides an additional charge storage mechanism (pseudocapacitance), the magnitude of which depends on the nature of the redox couple and the conductivity of the COFs. We evaluated these processes in the **DAAQ-TFP COF**, which offers both high surface area and surface-confined reversible redox processes, as compared to monomers **1** or **2** and the **DAB-TFP COF**, which lack high surface area and redox-active groups, respectively. An electrode functionalized only with carbon black and PVDF binder also showed only double-layer capacitive behavior under these conditions (Figure 4, blue), indicating that the Faradaic processes observed for **DAAQ-TFP COF** correspond to anthraquinone reduction and oxidation.

The **DAAQ-TFP COF** exhibits enhanced capacitance relative to monomers **1** and **2**, **DAB-TFP COF**, and carbon black, as determined by galvanostatic charge−discharge (GCDC) experiments (Figure 5). In a GCDC experiment, a constant current is applied to a sample and the potential is measured as a function of time. The charge polarity is reversed when the potential reaches a predetermined limit, such that one measurement cycle characterizes both the charging and discharging processes of the modified electrode under test. GCDC experiments of the **DAAQ-** and **DAB-TFP COF**, **1**, and **2**-functionalized electrodes at current densities of 0.1 A g^{-1} exhibit voltage−time profiles that reflect differences in their chemical composition and structure (GCDC experiments at increased charge density are provided in the SI). The monomer **2** and **DAB-TFP COF**-functionalized electrodes exhibit classic "shark-fin" GCDC profiles indicative of double-layer capacitance (Figure 5A). In contrast, GCDC profiles of the **DAAQ-TFP COF** and **DAAQ** monomer **1** display voltage plateaus at −0.05 V vs Ag/AgCl indicative of charge transfer to/from the anthraquinones. Capacitances derived from these measurements reflect the outstanding stability of the β-ketoenamine linkage of the **TFP**-based COFs, even in 1 M H_2SO_4 electrolyte. **DAAQ-TFP COF** modified electrodes initially provided a capacitance of 48 ± 10 F g^{-1}, which stabilized at 40 ± 9 F g^{-1} after 10 charge/discharge cycles, after which no further significant decrease was observed after 5000 cycles. The monomer **1** provides a lower initial capacitance (35 ± 7 F g^{-1}) and a more pronounced decrease upon cycling, stabilizing at 21 ± 3 F g^{-1}, ~60% of its initial capacitance. The **DAB-TFP COF** and **DAB** monomer **2**-modified electrodes also showed excellent

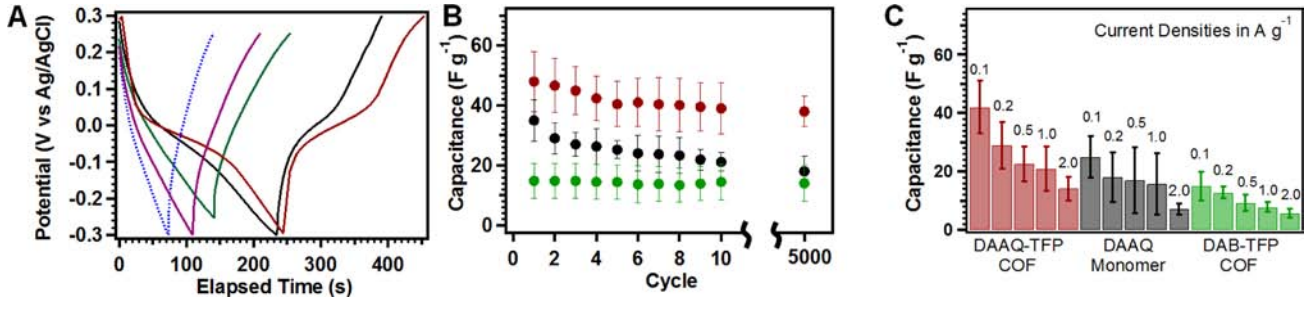

Figure 5. Representative galvanostatic charge−discharge response for **DAAQ-TFP COF** (red), monomer **1** (black), **DAB-TFP COF** (green), monomer **2** (purple), and a carbon black-only electrode (blue) at a current density of 0.1 A g^{-1}. (B) Average discharge capacitance (of 3 electrodes, error bars = ± 1 std. dev.) for **DAAQ-TFP COF** (red), monomer **1** (black), and **DAB-TFP COF** (green) at 0.1 A g^{-1} as a function of cycle number. (C) Plot of the average capacitances (of 3 electrodes, error bars = ± 1 std. dev.) of each electrode type at different applied current density.

dx.doi.org/10.1021/ja409421d | J. Am. Chem. Soc. 2013, 135, 16821−16824

stability, but similar overall capacitance (15 ± 6 and 13 ± 1 F g^{-1}, respectively) relative to an electrode comprised of carbon-black alone (12 ± 1 F g^{-1}). We estimated the accessible electroactive area of the **DAAQ-TFP COF** system by comparing the charge transferred to/from the anthraquinones in the CV experiment to its theoretical maximum based on the amount of COF adsorbed to the electrode. These calculations suggest that only 2.5% of the DAAQ moieties are accessed, which we attribute to the randomly oriented, polycrystalline **DAAQ-TFP COF** particles used in these electrodes. Therefore, we anticipate that significantly higher energy density (up to 31 W h kg^{-1}, see SI) and capacitance (311 F g^{-1}, see SI) might be achieved for COFs that are more conductive and are interfaced to the bulk electrode more effectively.

In conclusion, we have described a β-ketoenamine-linked 2D COF capable of reversible Faradaic processes. Exchange experiments performed on β-ketoenamine model compounds confirmed that they undergo dynamic exchange with free anilines to enable framework crystallization, despite their excellent hydrolytic stability. Refinement of the solvothermal growth conditions provided crystalline **DAAQ-TFP COF** samples with high surface area. We attribute the rapid redox processes of the **DAAQ-TFP COF's** anthraquinone groups to the 2D COF architecture, in which simultaneous electron and proton transfers can occur in the pores. As such, similar measurements of the monomer **1** exhibited sluggish charge-transfer kinetics as well as a shift in the formal potential for anthraquinone reduction. Electrodes functionalized with the **DAAQ-TFP COF** exhibit increased capacitance over those functionalized with either the **DAAQ** monomer **1** or the nonredox active monomer **2** and **DAB-TFP COF**. The exceptional stability of each β-ketoenamine-linked COF in H_2SO_4 electrolyte provided stable capacitances over at least 5000 charge−discharge cycles. These findings demonstrate the promise of β-ketoenamine-linked COFs for electrochemical energy storage devices, which will greatly benefit from synthesizing these materials as thin films on conductive substrates such that most of their redox-active groups might be accessed.

■ ASSOCIATED CONTENT

Ⓢ Supporting Information

Experimental procedures and characterization data. This material is available free of charge via the Internet at http://pubs.acs.org.

■ AUTHOR INFORMATION

Corresponding Author

wdichtel@cornell.edu

Notes

The authors declare no competing financial interest.

■ ACKNOWLEDGMENTS

This research was supported by the NSF in the form of CAREER (CHE-1056657) and NSF GRFP (DGE-1144153) awards to C.R.D., the Sloan Research Fellowship, and the Camille and Henry Dreyfus Foundation's Camille Dreyfus Teacher-Scholar Award. This research made use of the Cornell Center for Materials Research Facilities supported by the NSF (DMR-1120296). This work was supported in part (K.E.S., T.T.T., H.D.A.) by the DOE though grant DE-FG02-87ER45298, by the Energy Materials Center at Cornell, an Energy Frontier Research Center funded by the DOE Office of Basic Energy Sciences under award no. DE-SC0001086. K.E.S. was supported by a fellowship from the Cornell High Energy Synchrotron Source. T.T.T. was supported by an IGERT Fellowship (DGE-0903653). We thank Dr. Jason A. Mann and Mr. Abraham Saldivar for helpful discussions.

■ REFERENCES

(1) (a) Degani, Y.; Heller, A. *J. Phys. Chem.* **1987**, *91*, 1285−1289. (b) Ekanayake, E. M. I. M.; Preethichandra, D. M. G.; Kaneto, K. *Biosens. Bioelectron.* **2007**, *23*, 107−113.

(2) (a) Babu, K. F.; Kulandainathan, M. A.; Katsounaros, I.; Rassaei, L.; Burrows, A. D.; Raithby, P. R.; Marken, F. *Electrochem. Commun.* **2010**, *12*, 632−635. (b) Yang, L.; Kinoshita, S.; Yamada, T.; Kanda, S.; Kitagawa, H.; Tokunaga, M.; Ishimoto, T.; Ogura, T.; Nagumo, R.; Miyamoto, A.; Koyama, M. *Angew. Chem., Int. Ed.* **2010**, *49*, 5348−5351.

(3) (a) Winter, M.; Brodd, R. J. *Chem. Rev.* **2004**, *104*, 4245−4270. (b) Rauda, I. E.; Augustyn, V.; Dunn, B.; Tolbert, S. H. *Acc. Chem. Res.* **2013**, 1113−1124. (c) Thomas, A.; Kuhn, P.; Weber, J.; Titirici, M.-M.; Antonietti, M. *Macromol. Rapid Commun.* **2009**, *30*, 221−236.

(4) (a) Newman, J.; Tiedemann, W. *AlChE J.* **1975**, *21*, 25−41. (b) de Combarieu, G.; Morcrette, M.; Millange, F.; Guillou, N.; Cabana, J.; Grey, C. P.; Margiolaki, I.; Férey, G.; Tarascon, J.-M. *Chem. Mater.* **2009**, *21*, 1602−1611.

(5) (a) Chmiola, J.; Yushin, G.; Gogotsi, Y.; Portet, C.; Simon, P.; Taberna, P. L. *Science* **2006**, *313*, 1760−1763. (b) Stoller, M. D.; Ruoff, R. S. *Energy Environ. Sci.* **2010**, *3*, 1294. Stoller, M. D.; Stoller, S. A.; Quarles, N.; Suk, J. W.; Murali, S.; Zhu, Y.; Zhu, X.; Ruoff, R. S. *J. Appl. Electrochem.* **2011**, *41*, 681−686. (c) Merlet, C.; Rotenberg, B.; Madden, P. A.; Taberna, P.-L.; Simon, P.; Gogotsi, Y.; Salanne, M. *Nat. Mater.* **2012**, *11*, 306−310. (d) Lai, L.; Yang, H.; Wang, L.; Teh, B. K.; Zhong, J.; Chou, H.; Chen, L.; Chen, W.; Shen, Z.; Ruoff, R. S.; Lin, J. *ACS Nano* **2012**, *6*, 5941−5951. (e) Chen, W.; Rakhi, R. B.; Alshareef, H. N. *J. Mater. Chem.* **2012**, *22*, 14394−14402. (f) Hao, L.; Li, X.; Zhi, L. *Adv. Mater.* **2013**, *25*, 3899−3904.

(6) (a) Zhang, L. L.; Zhao, X.; Stoller, M. D.; Zhu, Y.; Ji, H.; Murali, S.; Wu, Y.; Perales, S.; Clevenger, B.; Ruoff, R. S. *Nano Lett.* **2012**, *12*, 1806−1812. (b) Wang, G.; Zhang, L.; Zhang, J. *Chem. Soc. Rev.* **2012**, *41*, 797−828.

(7) (a) Steele, B. C.; Heinzel, A. *Nature* **2001**, *414*, 345−352. (b) Virkar, A. *Solid State Ionics* **2000**, *131*, 189−198. (c) Yi, J. S. *J. Electrochem. Soc.* **1999**, *146*, 38−45.

(8) Choi, N. S.; Chen, Z.; Freunberger, S. A.; Ji, X.; Sun, Y. K.; Amine, K.; Yushin, G.; Nazar, L. F.; Cho, J.; Bruce, P. G. *Angew. Chem., Int. Ed.* **2012**, *51*, 9994−10024.

(9) Côté, A. P.; Benin, A. I.; Ockwig, N. W.; O'Keeffe, M.; Matzger, A. J.; Yaghi, O. M. *Science* **2005**, *310*, 1166−1170.

(10) (a) Colson, J. W.; Dichtel, W. R. *Nat. Chem.* **2013**, *5*, 453−65. (b) Feng, X.; Ding, X.; Jiang, D. *Chem. Soc. Rev.* **2012**, *41*, 6010−6022.

(11) (a) Wan, S.; Guo, J.; Kim, J.; Ihee, H.; Jiang, D. *Angew. Chem., Int. Ed.* **2009**, *48*, 5439−5442. (b) Ding, X.; Chen, L.; Honsho, Y.; Feng, X.; Saengsawang, O.; Guo, J.; Saeki, A.; Seki, S.; Irle, S.; Nagase, S.; Parasuk, V.; Jiang, D. *J. Am. Chem. Soc.* **2011**, *133*, 14510−14513.

(12) Kandambeth, S.; Mallick, A.; Lukose, B.; Mane, M. V.; Heine, T.; Banerjee, R. *J. Am. Chem. Soc.* **2012**, *134*, 19524−19527.

(13) Biswal, B. P.; Chandra, S.; Kandambeth, S.; Lukose, B.; Heine, T.; Banerjee, R. *J. Am. Chem. Soc.* **2013**, *135*, 5328−5331.

(14) Colson, J. W.; Woll, A. R.; Mukherjee, A.; Levendorf, M. P.; Spitler, E. L.; Shields, V. B.; Spencer, M. G.; Park, J.; Dichtel, W. R. *Science* **2011**, *332*, 228−231.

(15) Chong, J. H.; Sauer, M.; Patrick, B. O.; MacLachlan, M. J. *Org. Lett.* **2003**, *5*, 3823−38236.

(16) Farchioni, R. G. G. *Organic Electronic Materials: Conjugated Polymers and Low Molecular Weight Organic Solids*; Springer: Berlin, 2001.

(17) (a) Ding, S.-Y.; Gao, J.; Wang, Q.; Zhang, Y.; Song, W.-G.; Su, C.-Y.; Wang, W. *J. Am. Chem. Soc.* **2011**, *133*, 19816−19822. (b) Nagai, A.; Chen, X.; Feng, X.; Ding, X.; Guo, Z.; Jiang, D. *Angew. Chem., Int. Ed.* **2013**, *52*, 3770−3774.